THE JOURNAL
OF THE
ACOUSTICAL SOCIETY OF AMERICA

Volume 23 Number 4

JULY • 1951

Sound Scattering by Solid Cylinders and Spheres*

JAMES J. FARAN, JR.
Acoustics Research Laboratory, Harvard University, Cambridge, Massachusetts
(Received March 13, 1951)

The theory of the scattering of plane waves of sound by isotropic circular cylinders and spheres is extended to take into account the shear waves which can exist (in addition to compressional waves) in scatterers of solid material. The results can be expressed in terms of scattering functions already tabulated. Scattering patterns computed on the basis of the theory are shown to be in good agreement with experimental measurements of the distribution-in-angle of sound scattered in water by metal cylinders. Rapid changes with frequency in the distribution-in-angle of the scattered sound and in the total scattered energy are found to occur near frequencies of normal modes of free vibration of the scattering body.

I. INTRODUCTION

THE scattering of sound was first investigated mathematically by Lord Rayleigh.[1] However, because of the complexity of the mathematical solution, he only considered the limiting case where the scatterers are small compared with the wavelength. The solution for scattering by rigid, immovable circular cylinders and spheres, not necessarily small compared with the wavelength, was given in convenient form by Morse, who defined and tabulated values of phase-angles associated with the partial scattered waves, in order to simplify the complicated dependence on bessel functions.[2] Although most solid scatterers in air can be considered rigid and immovable, it is valid only in a few special cases to assume that a scatterer in a liquid medium is rigid and immovable. In general, the sound waves which penetrate the scatterer must be taken into account, as they can have a considerable effect on the distribution-in-angle of the scattered sound and on the total scattered energy. Morse, with Lowan, Feshbach, and Lax, later extended his solution to include the effects of compressional waves inside (fluid) cylindrical and spherical scatterers.[3] These results are also given in convenient form in terms of several additional phase-angles whose values are tabulated. The object of the research reported here has been to study sound scattering by cylinders and spheres of solid material (which will support shear waves in addition to compressional waves). The mathematical solution will be given first, after which experimental apparatus and results will be described.

II. THE MATHEMATICAL SOLUTION

List of Symbols

Most of the symbols used here are, in the appropriate sections of the analysis, the same as those used by Love and those used by Morse:

a = radius of cylinder or sphere;
a_n, b_n, c_n = expansion coefficients;

* This paper contains the essential results of a thesis submitted to the Faculty of Harvard University in partial fulfillment of the requirements for the degree of Doctor of Philosophy. This research has been aided by funds made available under a contract with the ONR.

[1] Lord Rayleigh, *The Theory of Sound* (Dover Publications, New York, 1945), first American edition.

[2] P. M. Morse, *Vibration and Sound* (McGraw-Hill Book Company, New York, 1936), first edition, and (1948), second edition.

[3] Mathematical Tables Project and M.I.T. Underwater Sound Laboratory, *Scattering and Radiation from Circular Cylinders and Spheres* (U. S. Navy Department, Office of Research and Inventions, Washington, D. C., 1946).

$\mathbf{A}$ = vector displacement potential;
A_z = z-component of vector potential;
A_ϕ = ϕ-component of vector potential;
c_1 = velocity of compressional waves in the scatterer;
c_2 = velocity of shear waves in the scatterer;
c_3 = velocity of sound in the fluid surrounding the scatterer;
E = Young's modulus;
j = $(-1)^{\frac{1}{2}}$;
$j_n(\ )$ = spherical bessel function of the first kind;
$J_n(\ )$ = bessel function of the first kind;
k_1 = ω/c_1;
k_2 = ω/c_2;
k_3 = ω/c_3;
n = order integer;
$n_n(\ )$ = spherical bessel function of the second kind;
$N_n(\ )$ = bessel function of the second kind;
p = pressure;
p_i = pressure in incident wave;
p_s = pressure in scattered wave;
$P_n(\cos\theta)$ = Legendre polynomial;
P_0 = amplitude of pressure in incident wave;
r, θ, z = cylindrical coordinates;
r, θ, ϕ = spherical coordinates;
$[rr], [r\theta], [rz]$ = stress components in cylindrical coordinates;
$[rr], [r\theta], [r\phi]$ = stress components in spherical coordinates;
t = time;
$\mathbf{u}$ = displacement;
u_r, u_θ = components of displacement in the solid;
$u_{i,r}$ = radial component of displacement in incident wave;
$u_{s,r}$ = radial component of displacement in scattered wave;
x, y, z = rectangular coordinates;
x_1 = $k_1 a$;
x_2 = $k_2 a$;
x_3 = $k_3 a$;
$\alpha_n, \beta_n, \delta_n, \delta_n', \zeta_n, \eta_n$ = scattering phase-angles;
Δ = dilatation;
ϵ_n = Neumann factor; $\epsilon_0=1$; $\epsilon_n=2$, $n>0$;
λ, μ = Lamé elastic constants;
$2\tilde{\omega}$ = rotation;
ρ_1 = density of the scatterer;
ρ_3 = density of the fluid surrounding the scatterer;
σ = Poisson's ratio;
Φ_n = boundary impedance scattering phase-angle;
Ψ = scalar displacement potential;
ω = angular frequency $(2\pi f)$.

Scattering by Solid Circular Cylinders

Plane waves of sound of frequency $\omega/2\pi$ in a fluid medium are incident upon an infinitely long circular cylinder of some isotropic solid material. Let the axis of the cylinder coincide with the z-axis of a rectangular coordinate system, and let the plane wave approach the cylinder along the negative x-axis, as shown in Fig. 1. As in the solutions given previously for rigid and fluid scatterers,[1–3] the wave motion external to the scatterer is assumed to consist of the incident plane wave and an outgoing scattered wave. It is desired to find the amplitude of the scattered wave as measured at large distances from the cylinder. The mathematical expressions for displacement and dilatation inside and for pressure and displacement outside the cylinder will be found in general form first, after which the application of the proper boundary conditions at the surface of the cylinder will lead directly to the solution.

The waves inside the cylinder will be represented by suitable solutions of the equation of motion of a solid elastic medium, which may be written[4]

$$(\lambda+2\mu)\nabla\Delta-\mu\nabla\times(2\tilde{\omega})=\rho_1\partial^2\mathbf{u}/\partial t^2, \tag{1}$$

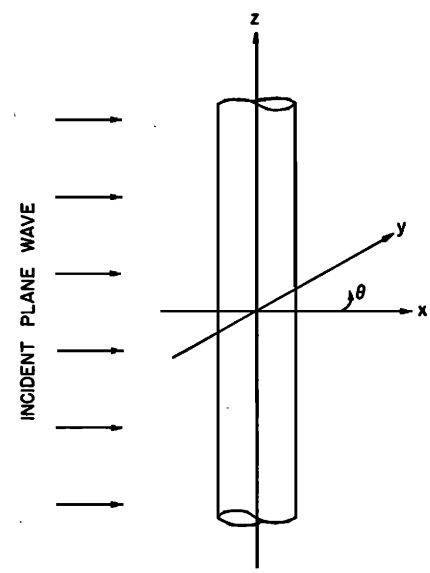

FIG. 1. Choice of coordinate axes for scattering by cylinders.

where

$$\Delta=\nabla\cdot\mathbf{u} \tag{2}$$

and

$$2\tilde{\omega}=\nabla\times\mathbf{u}.$$

From Eq. (1) can be derived the equations,

$$\nabla^2\Delta=(\rho_1/\lambda+2\mu)\partial^2\Delta/\partial t^2 \tag{3}$$

and

$$\nabla^2(2\tilde{\omega})=(\rho_1/\mu)\partial^2(2\tilde{\omega})/\partial t^2, \tag{4}$$

which define the wave velocities

$$c_1=[(\lambda+2\mu)/\rho_1]^{\frac{1}{2}}=[E(1-\sigma)/\rho_1(1+\sigma)(1-2\sigma)]^{\frac{1}{2}} \tag{5}$$

and

$$c_2=(\mu/\rho_1)^{\frac{1}{2}}=[E/2\rho_1(1+\sigma)]^{\frac{1}{2}}. \tag{6}$$

Solutions of Eq. (1) can be found by assuming that the

[4] A. E. H. Love, *A Treatise on the Mathematical Theory of Elasticity* (Dover Publications, New York, 1944), fourth edition, p. 141.

displacement can be derived from a scalar and a vector potential:

$$\mathbf{u}=-\nabla\Psi+\nabla\times\mathbf{A}. \tag{7}$$

The displacement thus can be thought of as the sum of two displacements, one associated with compressional waves and the other with shear waves. If we assume that the potentials satisfy the equations,

$$\nabla^2\Psi=(1/c_1^2)\partial^2\Psi/\partial t^2 \tag{8}$$

and

$$\nabla^2\mathbf{A}=(1/c_2^2)\partial^2\mathbf{A}/\partial t^2, \tag{9}$$

we can show that $\Delta(=\nabla\cdot(-\nabla\Psi))$ satisfies Eq. (3), and that $2\tilde{\omega}(=\nabla\times\nabla\times\mathbf{A})$ satisfies Eq. (4). That these assumptions do lead to a valid solution of Eq. (1) may be seen by noting that the solutions we shall obtain satisfy Eq. (1) by direct substitution. If we now change to a cylindrical coordinate system defined by

$$x=r\cos\theta,\quad y=r\sin\theta,\quad z=z,$$

it can be seen that pressure and displacement must be symmetrical about $\theta=0$ (the direction of the positive x-axis). Moreover, because the cylinder is of infinite length, and the incident plane wave of infinite extent, there can be no dependence on z, and it is logical to assume that there is no displacement in the z-direction. Subject to these conditions, the solution of Eq. (8) can be written

$$\Psi=\sum_{n=0}^{\infty}a_nJ_n(k_1r)\cos n\theta. \tag{10}$$

(The time dependence factor $\exp(j\omega t)$ will be understood in all the expressions representing waves.) Examination of Eq. (9) shows that, subject to the conditions discussed above, the vector potential can have no component in the r- or the θ-direction. The vector Eq. (9) then reduces to a scalar equation in A_z, and its solution can be written

$$A_z=\sum_{n=0}^{\infty}b_nJ_n(k_2r)\sin n\theta. \tag{11}$$

Only sine terms appear here, because the vector potential must be anti-symmetrical about $\theta=0$ in order that the displacement derived from it shall be symmetrical about $\theta=0$. Now, by Eqs. (7) and (2),

$$u_r=\sum_{n=0}^{\infty}\left[\frac{nb_n}{r}J_n(k_2r)-a_n\frac{d}{dr}J_n(k_1r)\right]\cos n\theta, \tag{12}$$

$$u_\theta=\sum_{n=0}^{\infty}\left[\frac{na_n}{r}J_n(k_1r)-b_n\frac{d}{dr}J_n(k_2r)\right]\sin n\theta, \tag{13}$$

and

$$\Delta=k_1^2\sum_{n=0}^{\infty}a_nJ_n(k_1r)\cos n\theta. \tag{14}$$

The waves in the fluid surrounding the cylinder will be represented by suitable solutions of the wave equation for a (nonviscous) fluid medium, which can be written

$$\nabla^2p=(1/c_3^2)\partial^2p/\partial t^2.$$

The incident plane wave is represented by[5]

$$\begin{aligned}p_i&=P_0\exp(-jk_3x)=P_0\exp(-jk_3r\cos\theta)\\&=P_0\sum_{n=0}^{\infty}\epsilon_n(-j)^nJ_n(k_3r)\cos n\theta.\end{aligned} \tag{15}$$

The radial component of displacement associated with this wave is

$$\begin{aligned}u_{i,r}&=(1/\rho_3\omega^2)\partial p_i/\partial r\\&=\frac{P_0}{\rho_3\omega^2}\sum_{n=0}^{\infty}\epsilon_n(-j)^n\frac{d}{dr}J_n(k_3r)\cos n\theta.\end{aligned} \tag{16}$$

The outgoing scattered wave must be symmetrical about $\theta=0$ and therefore of the form

$$p_s=\sum_{n=0}^{\infty}c_n[J_n(k_3r)-jN_n(k_3r)]\cos n\theta. \tag{17}$$

The radial component of displacement associated with this wave is

$$u_{s,r}=\frac{1}{\rho_3\omega^2}\sum_{n=0}^{\infty}c_n\frac{d}{dr}[J_n(k_3r)-jN_n(k_3r)]\cos n\theta. \tag{18}$$

The factors c_n are the unknown coefficients which must be evaluated.

The following boundary conditions are applied at the surface of the cylinder: (I) The pressure in the fluid must be equal to the normal component of stress in the solid at the interface; (II) the normal (radial) component of displacement of the fluid must be equal to the normal component of displacement of the solid at the interface; and (III) the tangential components of shearing stress must vanish at the surface of the solid. That is,

$$p_i+p_s=-[rr]\quad\text{at}\quad r=a, \tag{19}$$

$$u_{i,r}+u_{s,r}=u_r\qquad\text{at}\quad r=a, \tag{20}$$

and

$$[r\theta]=[rz]=0\quad\text{at}\quad r=a. \tag{21}$$

In cylindrical coordinates,[6]

$$[rr]=\lambda\Delta+2\mu\partial u_r/\partial r=2\rho_1c_2^2[(\sigma/1-2\sigma)\Delta+\partial u_r/\partial r],$$
$$[r\theta]=\mu[(1/r)(\partial u_r/\partial\theta)+(r\partial/\partial r)(u_\theta/r)],$$

and

$$[rz]=\mu[\partial u_r/\partial z+\partial u_z/\partial r].$$

By the conditions of symmetry, $[rz]=0$ everywhere. Upon substitution from Eqs. (15), (17), (14), (12), (16), (18), and (13), the boundary condition Eqs. (19), (20),

[5] See reference 2, second edition, p. 347.
[6] See reference 4, p. 288.

and (21) become, for the nth mode,

$$x_1J_n'(x_1)a_n-nJ_n(x_2)b_n+(x_3/\omega^2\rho_3)[J_n'(x_3)-jN_n'(x_3)]c_n=-(P_0x_3/\omega^2\rho_3)\epsilon_n(-j)^nJ_n'(x_3), \quad (19a)$$

$$2\rho_1c_2^2x_1^2[(\sigma/1-2\sigma)J_n(x_1)-J_n''(x_1)]a_n+2\rho_1c_2^2n[x_2J_n'(x_2)-J_n(x_2)]b_n+a^2[J_n(x_3)-jN_n(x_3)]c_n=-P_0\epsilon_n(-j)^na^2J_n(x_3), \quad (20a)$$

and

$$2n[x_1J_n'(x_1)-J_n(x_1)]a_n=[n^2J_n(x_2)-x_2J_n'(x_2)+x_2^2J_n''(x_2)]b_n. \quad (21a)$$

Solving these equations simultaneously for c_n is laborious but straightforward. The result is

$$c_n=-P_0\epsilon_n(-j)^{n+1}\sin\eta_n\exp(j\eta_n), \quad (22)$$

where η_n, the phase-shift angle of the nth scattered wave, is defined by

$$\tan\eta_n=\tan\delta_n(x_3)\times[\tan\Phi_n+\tan\alpha_n(x_3)]/[\tan\Phi_n+\tan\beta_n(x_3)].$$

The intermediate scattering phase-angles

$$\delta_n(x)=\tan^{-1}[-J_n(x)/N_n(x)],$$
$$\alpha_n(x)=\tan^{-1}[-xJ_n'(x)/J_n(x)],$$

and

$$\beta_n(x)=\tan^{-1}[-xN_n'(x)/N_n(x)],$$

have been defined and their values tabulated previously.[3] The angle Φ_n, which is a measure of the boundary impedance at the surface of the scatterer, is given, for a solid scatterer, by

$$\tan\Phi_n=(-\rho_3/\rho_1)\tan\zeta_n(x_1,\sigma), \quad (23)$$

where the new scattering phase-angle $\zeta_n(x_1,\sigma)$ is given by

$$\zeta_n(x_1,\sigma)=\tan^{-1}\left[-\frac{x_2^2}{2}\frac{\dfrac{x_1J_n'(x_1)}{x_1J_n'(x_1)-J_n(x_1)}-\dfrac{2n^2J_n(x_2)}{n^2J_n(x_2)-x_2J_n'(x_2)+x_2^2J_n''(x_2)}}{\dfrac{(\sigma/1-2\sigma)x_1^2[J_n(x_1)-J_n''(x_1)]}{x_1J_n'(x_1)-J_n(x_1)}+\dfrac{2n^2[x_2J_n'(x_2)-J_n(x_2)]}{n^2J_n(x_2)-x_2J_n'(x_2)+x_2^2J_n''(x_2)}}\right]. \quad (24)$$

For convenience in computing values of this function, it can be written in terms of the angle $\alpha_n(x)$:

$$\zeta_n(x_1,\sigma)=\tan^{-1}\left[-\frac{x_2^2}{2}\frac{\dfrac{\tan\alpha_n(x_1)}{\tan\alpha_n(x_1)+1}-\dfrac{n^2}{\tan\alpha_n(x_2)+n^2-\frac{1}{2}x_2^2}}{\dfrac{\tan\alpha_n(x_1)+n^2-\frac{1}{2}x_2^2}{\tan\alpha_n(x_1)+1}-\dfrac{n^2[\tan\alpha_n(x_2)+1]}{\tan\alpha_n(x_2)+n^2-\frac{1}{2}x_2^2}}\right]. \quad (25)$$

Although ζ_n as written above is explicitly a function of x_1 and x_2, it can be considered a function of x_1 and σ, since the ratio of x_1 and x_2 is a function of σ only. Values of $\zeta_n(x_1,\sigma)$ computed from Eq. (25) for $\sigma=\frac{1}{3}$ are given in Table I. For convenience in finding the tangent, the value of the angle lying between $\pm90°$ is given in the table. The dotted lines indicate that $\zeta_n(x_1,\sigma)$ passes through $\pm90°$ between the adjacent entries, and thus serve to point out the infinities of $\tan\zeta_n(x_1,\sigma)$. It will be seen below that the infinities of $\tan\zeta_n(x_1,\sigma)$ occur at precisely the frequencies of those normal modes of free vibration of the scatterer which satisfy the conditions of symmetry of the scattering problem. The dotted lines in Table I thus mark the locations of the normal modes of vibration of the scatterer. For other values of Poisson's ratio the functions will be similar, the only difference being shifts in the locations of the normal modes.

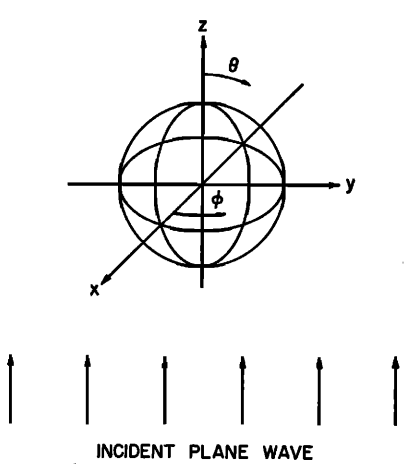

FIG. 2. Choice of coordinate axes for scattering by spheres.

The scattering pattern, or distribution-in-angle of pressure in the scattered wave at large distances from the cylinder, can be found from Eqs. (17) and (22), using the asymptotic expressions for the bessel functions for large arguments:

$$|p_s|\underset{r\to\infty}{\longrightarrow}P_0\left(\frac{2}{\pi k_3r}\right)^{\frac{1}{2}}\left|\sum_{n=0}^{\infty}\epsilon_n\sin\eta_n\exp(j\eta_n)\cos n\theta\right|. \quad (26)$$

Scattering by Solid Spheres

Let us assume that plane waves of sound in a fluid medium are incident upon a sphere of some isotropic

TABLE I. Values of $\zeta_n(x_1, \sigma)$ for the cylindrical case for $\sigma=\frac{1}{3}$.

x_1	$n=0$	$n=1$	$n=2$	$n=3$	$n=4$	$n=5$	$n=6$	$n=7$	$n=8$	$n=9$
0.0	0.00°	−45.00°	0.00°	0.00°	0.00°	0.00°	0.00°	0.00°	0.00°	0.00°
0.2	1.37	−44.13	3.59	2.06	1.52	1.20	1.01	0.86	0.76	0.67
0.4	6.27	−43.33	15.47	8.73	6.33	4.97	4.02	3.46	3.03	2.68
0.6	14.35	−41.18	36.24	20.10	14.07	11.15	9.12	7.80	6.80	6.04
0.8	25.60	−37.48	60.28	35.26	25.40	19.90	16.24	14.00	12.12	10.24
1.0	38.90	−31.24	79.03	51.42	37.95	30.52	25.18	21.23	18.52	16.84
1.2	52.22	−18.06	·····	65.40	50.79	41.33	34.96	30.31	26.58	23.56
1.4	63.81	+62.49	−88.71	76.03	61.87	52.07	45.11	38.96	34.61	31.22
1.6	73.08	·····	−31.82	−74.29	83.85	70.71	61.11	53.83	47.93	42.73	39.11
1.8	80.33	−7.53	−68.94	89.73	77.52	68.61	61.51	55.74	50.71	46.45
2.0	86.05	+15.39	−63.54	·····	−85.59	82.84	74.55	67.96	62.24	57.38	53.06
2.2	·····	−89.25	36.63	−56.21	−81.57	87.06	79.25	73.05	67.88	63.03	59.43
2.4	−85.16	53.17	·····	−49.71	−77.67	·····	−89.43	83.05	77.21	72.25	67.97	64.10
2.6	−81.30	64.93	−37.81	−73.08	−86.35	86.22	80.71	76.15	72.17	68.51
2.8	−77.32	73.30	−19.43	−64.48	−83.42	88.92	83.58	79.25	75.52	72.15
3.0	−72.71	79.69	+6.92	+68.10	−80.28	·····	−88.67	86.02	81.83	78.34	75.20
3.2	−66.65	85.83	34.29	·····	−74.64	−76.17	−86.39	88.15	84.09	80.71	77.75
3.4	−57.35	·····	74.49	54.21	−65.75	−68.06	−84.05	·····	−89.92	86.04	82.78	79.94
3.6	−40.29	87.38	67.25	−55.95	−11.94	−81.35	−88.10	87.77	84.58	81.86
3.8	−6.92	·····	−89.02	76.96	−40.24	+85.24	−77.55	−86.28	89.35	86.18	83.57
4.0	+34.15	−86.10	·····	−87.62	−11.45	·····	−83.85	−69.80	−84.30	·····	−89.16	87.59	85.03
4.2	58.25	−83.24	+70.33	+28.36	−78.33	−27.54	−81.87	−87.69	88.91	86.34
4.4	70.32	−80.06	80.59	57.79	−73.27	+75.02	−78.22	−86.15	·····	−89.85	87.54
4.6	77.19	−76.03	84.69	78.81	−66.94	88.55	−70.46	−84.38	−88.63	88.64
4.8	81.68	−70.05	87.52	·····	14.69	−56.75	·····	−86.36	−29.41	−82.10	−87.38	89.69
5.0	84.94	−60.60	89.87	68.66	−34.99	−82.97	+70.97	−78.49	−86.02	·····	−89.28

solid material. Let the center of the sphere coincide with the origin of a rectangular coordinate system, and let the plane waves approach the sphere along the negative z axis, as shown in Fig. 2. The analysis is very similar to that for the cylindrical case. We transfer to spherical coordinates defined by

$$x=r\sin\theta\cos\phi, \quad y=r\sin\theta\sin\phi, \quad z=r\cos\theta.$$

Because the incident wave approaches along the axis of ϕ, there is no dependence on ϕ. It is logical to assume that there is no component of displacement in the ϕ-direction, and it follows that the only non-zero component of the vector potential in this case is A_ϕ. The potentials are then found to be of the forms,

$$\Psi=\sum_{n=0}^{\infty} a_n j_n(k_1 r)P_n(\cos\theta)$$

and

$$A_\phi=\sum_{n=0}^{\infty} b_n j_n(k_2 r)\frac{d}{d\theta}P_n(\cos\theta).$$

Pressure in the incident wave is represented by[7]

$$p_i=P_0\exp(-jk_3 z)=P_0\exp(-jk_3 r\cos\theta)$$

$$=P_0\sum_{n=0}^{\infty}(2n+1)(-j)^n j_n(k_3 r)P_n(\cos\theta).$$

The outgoing scattered wave will be of the form,

$$p_s=\sum_{n=0}^{\infty} c_n[j_n(k_3 r)-jn_n(k_3 r)]P_n(\cos\theta). \qquad (27)$$

The same boundary conditions at the surface of the scatterer are applied to the expressions for displacement, pressure, and dilatation, which are either given above or derivable from the above. In spherical coordinates the stress components are

$$[rr]=\lambda\Delta+2\mu\partial u_r/\partial r=2\rho_1 c_2^2[(\sigma/1-2\sigma)\Delta+\partial u_r/\partial r],$$

$$[r\theta]=\mu\left[\frac{\partial u_\theta}{\partial r}-\frac{u_\theta}{r}+\frac{1}{r}\frac{\partial u_r}{\partial\theta}\right],$$

[7] See reference 2, second edition, p. 354.

and

$$[r\phi]=\mu\left[\frac{1}{r\sin\theta}\frac{\partial u_r}{\partial\theta}+\frac{\partial u_\phi}{\partial r}-\frac{u_\phi}{r}\right].$$

By carrying the analysis through as in the cylindrical case, we find that

$$c_n=-P_0(2n+1)(-j)^{n+1}\sin\eta_n\exp(j\eta_n), \quad (28)$$

where the phase-shift η_n of the nth scattered wave is defined by

$$\tan\eta_n=\tan\delta_n(x_3)[\tan\Phi_n+\tan\alpha_n(x_3)]/\tan\Phi_n+\tan\beta_n(x_3).$$

The intermediate angles,

$$\delta_n(x)=\tan^{-1}[-j_n(x)/n_n(x)],$$
$$\alpha_n(x)=\tan^{-1}[-xj_n'(x)/j_n(x)],$$
$$\beta_n(x)=\tan^{-1}[-xn_n'(x)/n_n(x)],$$

have been defined and their values tabulated previously.[8] The boundary impedance phase-angle Φ_n is defined by

$$\tan\Phi_n=-(\rho_3/\rho_1)\tan\zeta_n(x_1,\sigma), \quad (29)$$

where the new scattering phase angle $\zeta_n(x_1,\sigma)$ is given by

$$\zeta_n(x_1,\sigma)=\tan^{-1}\left[-\frac{x_2^2}{2}\frac{\dfrac{x_1j_n'(x_1)}{x_1j_n'(x_1)-j_n(x_1)}-\dfrac{2(n^2+n)j_n(x_2)}{(n^2+n-2)j_n(x_2)+x_2^2j_n''(x_2)}}{\dfrac{(\sigma/1-2\sigma)x_1^2[j_n(x_1)-j_n''(x_1)]}{x_1j_n'(x_1)-j_n(x_1)}-\dfrac{2(n^2+n)[j_n(x_2)-x_2j_n'(x_2)]}{(n^2+n-2)j_n(x_2)+x_2^2j_n''(x_2)}}\right].$$

This function can be expressed in terms of the angle $\alpha_n(x)$:

$$\zeta_n(x_1,\sigma)=\tan^{-1}\left[-\frac{x_2^2}{2}\frac{\dfrac{\tan\alpha_n(x_1)}{\tan\alpha_n(x_1)+1}-\dfrac{n^2+n}{n^2+n-1-\frac{1}{2}x_2^2+\tan\alpha_n(x_2)}}{\dfrac{n^2+n-\frac{1}{2}x_2^2+2\tan\alpha_n(x_1)}{\tan\alpha_n(x_1)+1}-\dfrac{(n^2+n)[\tan\alpha_n(x_2)+1]}{n^2+n-1-\frac{1}{2}x_2^2+\tan\alpha_n(x_2)}}\right]. \quad (30)$$

Values of this function computed from Eq. (30) for $\sigma=\frac{1}{3}$ are given in Table II. The dotted lines again indicate the infinities of $\tan\zeta_n(x_1,\sigma)$, that is, the normal modes of free vibration of the scatterer.

The distribution in angle of pressure in the scattered wave at large distances from the sphere is found from Eqs. (27) and (28) by means of the asymptotic expressions for the spherical bessel functions for large arguments:

$$|p_s|\underset{r\to\infty}{\rightarrow}\frac{P_0}{k_3r}\left|\sum_{n=0}^{\infty}(2n+1)\sin\eta_n\exp(j\eta_n)P_n(\cos\theta)\right|. \quad (31)$$

III. EXPERIMENTAL APPARATUS

Measurements of the distribution-in-angle of sound scattered in water by metal cylinders were made for the purpose of checking the theory. These measurements were made in a large steel tank at or near a frequency of one megacycle per second. A sound projector in one end of the tank irradiated the scatterer with sound. A receiving hydrophone was mounted in such a way that it could easily be moved to any position lying on a circle concentric with the scatterer, and served to measure the distribution in angle of the pressure in the scattered wave. Short wave trains or "pulses" of sound were used in order that the measurement of each pulse could be effectively completed before sound reflected from the walls of the tank could reach the receiving hydrophone. A novel feature, frequency modulation of the pulse repetition rate, served to identify interfering pulses which, still reverberating in the tank from the previous transmitted pulse, happened to arrive at the receiver at the same time as the pulse to be measured. A small adjustment of the average pulse repetition rate was effective in controlling interference of this type. Both transducers employed x-cut quartz crystals operated at resonance. Serious distortion of the short (64 μsec) pulses by the transducers was prevented by lowering the Q of the quartz crystals by increasing the radiation loading. This was accomplished by inserting between the crystals and the water an acoustic quarter-wave transformer in the form of a thin disk of Plexiglas. The amplitude of the scattered sound pulses was measured by a modified substitution method, an oscilloscope being used as an indicator. The pulses were brought to a standard deflection on the oscilloscope, changes in the pulse amplitude being compensated by changes in the attenuation in the receiving system.

IV. COMPARISON OF THEORY AND EXPERIMENT

The experimental data were normalized so that they could be compared with scattering patterns computed from the theory. In order to do this, the amplitude of the pressure in the incident wave (P_0) was measured by moving the receiving transducer to the position of the

[8] See reference 3. Care must be taken to distinguish between the cylindrical and spherical cases, since the same symbols are used for the scattering phase-angles in both cases.

TABLE II. Values of $\zeta_n(x_1, \sigma)$ for the spherical case for $\sigma=\frac{1}{3}$.

x_1	$n=0$	$n=1$	$n=2$	$n=3$	$n=4$	$n=5$	$n=6$	$n=7$	$n=8$	$n=9$
0.0	0.00°	−45.00°	0.00°	0.00°	0.00°	0.00°	0.00°	0.00°	0.00°	0.00°
0.2	1.16	−44.72	3.05	1.94	1.41	1.13	0.96	0.81	0.73	0.64
0.4	4.66	−43.57	12.77	7.77	5.91	4.66	3.91	3.33	2.93	2.62
0.6	10.58	−41.62	29.97	17.88	13.38	10.38	8.73	7.50	6.58	5.88
0.8	18.89	−38.54	51.40	31.55	23.47	18.83	15.93	13.58	12.19	11.01
1.0	29.12	−33.76	70.41	46.79	35.44	28.67	24.25	20.74	18.32	16.09
1.2	40.28	−26.18	83.89	60.52	47.88	39.29	33.22	29.67	25.84	23.32
1.4	51.05	−12.80	····· −86.94	71.44	58.67	50.00	43.23	38.34	34.49	31.51
1.6	60.55	+16.87	−80.31	79.64	67.68	59.02	52.20	46.57	42.41	38.72
1.8	68.41	89.15	−75.00	85.78	74.68	66.42	59.69	54.53	49.80	45.77
2.0	74.78	····· −25.58	−70.20	····· −89.46	80.14	72.50	66.17	60.82	56.28	52.29
2.2	79.92	+9.84	−65.27	−85.58	84.46	77.29	71.50	66.61	62.27	58.30
2.4	84.14	30.55	−59.50	−82.18	87.97	81.17	75.75	71.13	67.13	63.16
2.6	87.71	48.97	····· −52.57	−78.94	····· −89.07	84.39	79.27	74.89	71.11	67.61
2.8	····· −89.15	61.45	−41.61	−75.41	−86.44	87.06	82.18	78.10	74.62	71.07
3.0	−86.24	70.09	−25.03	−70.56	−83.95	89.38	84.63	80.80	77.41	74.43
3.2	−83.36	76.48	−0.51	−55.48	−81.37	····· −88.53	86.75	83.03	79.87	77.00
3.4	−80.31	81.81	+27.37	····· −81.31	−78.27	−86.56	88.61	84.98	81.93	79.23
3.6	−76.72	88.64	49.05	−68.79	−73.44	−84.57	····· −89.70	86.69	83.75	81.23
3.8	−72.00	····· 75.11	63.24	−59.85	−59.37	−82.35	−88.10	88.21	85.33	82.88
4.0	−64.84	85.64	72.99	−47.06	+65.07	−79.48	−86.50	89.61	86.71	84.30
4.2	−51.66	89.00	81.77	−24.13	····· −87.41	−74.70	−84.81	····· −89.07	87.99	85.62
4.4	−22.39	····· −88.45	····· −65.12	+13.38	−80.54	−60.64	−82.81	−87.76	89.17	86.81
4.6	+26.20	−86.12	+73.10	47.64	−75.60	+48.49	−80.07	−86.41	····· −89.71	87.88
4.8	56.58	−83.70	80.80	68.81	−70.16	84.65	−75.21	−84.90	−88.62	88.89
5.0	70.03	−80.89	84.41	····· −88.10	−62.36	····· −88.16	−60.25	−83.03	−87.50	89.85

scatterer. After normalization, it was still necessary to add a factor amounting to 1.9 db to the amplitude of the scattered sound in order to bring the experimental data into good agreement with the theory. This correction factor has been explained, and its value computed with good accuracy, by taking into account the fact that the illumination of the scatterer varies in phase and amplitude along its length.[9]

The part of Eq. (26) which was evaluated in computing the patterns was

$$\tfrac{1}{2}\Big|\sum_{n=0}^{\infty}\epsilon_n \sin\eta_n \exp(j\eta_n)\cos n\theta\Big|,$$

and the corresponding numerical scale is shown on all the patterns used as illustrations. The values of Poisson's ratio for the various scatterers were assumed, because of the difficulty of measuring this constant directly; but the values of Young's modulus were measured (to within ±5 percent) by finding the frequency of the first mode of flexual vibration of the cylindrical specimen mounted so that it could vibrate as a fixed-free bar. The value of x_1 was then determined by means of Eq. (5). In some cases where the pattern was very sensitive to frequency, it was necessary to choose a value of x_1 slightly different from that based on the Young's modulus measurement in order to bring the measured and computed patterns into agreement. Comparison of the value of Young's modulus corresponding to the assumed value of x_1 with the measured value serves in these cases to indicate the degree of agreement between experiment and theory.

Figures 3 through 13 are measured and computed scattering patterns for cylinders of various sizes. The pressure in the scattered wave is plotted linearly against scattering angle. In each case the arrow indicates the direction of the incident sound. The angle θ is measured from the top center of the graph, the incident sound coming from the direction $\theta=180°$. For each size of

[9] J. J. Faran, Jr., *Sound Scattering by Solid Cylinders and Spheres*, Technical Memorandum No. 22 (March 15, 1951), Acoustics Research Laboratory, Harvard University, Cambridge, Massachusetts.

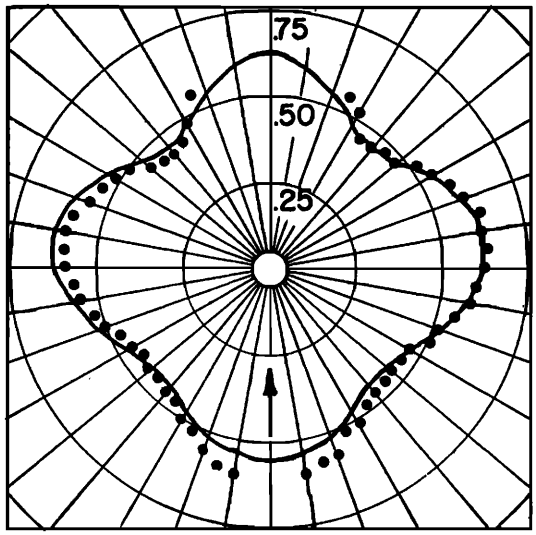

FIG. 3. Scattering pattern for brass cylinder 0.0322 in. in diameter at 1.00 mc/sec. *Points:* Measured amplitude of pressure in the scattered wave. The measured Young's modulus was 10.1 $\times 10^{11}$ dynes/cm^2. *Curve:* Computed pattern for $x_3=1.7$, $x_1=0.6$, $\sigma=\frac{1}{3}$, $\rho_1=8.5$ g/cm^3.

scatterer, the pattern computed on the basis that the scatterer is rigid and immovable is included for comparison.

Figures 3 and 4 show scattering patterns for brass and steel (drill rod) cylinders of the same size, for each of which $x_3=1.7$. These patterns are both very similar to that for a rigid, immovable scatterer of the same size (Fig. 5).

Figures 6–8 show scattering patterns for cylinders of various materials twice as large in diameter, that is, $x_3=3.4$. The pattern for a brass cylinder of this size

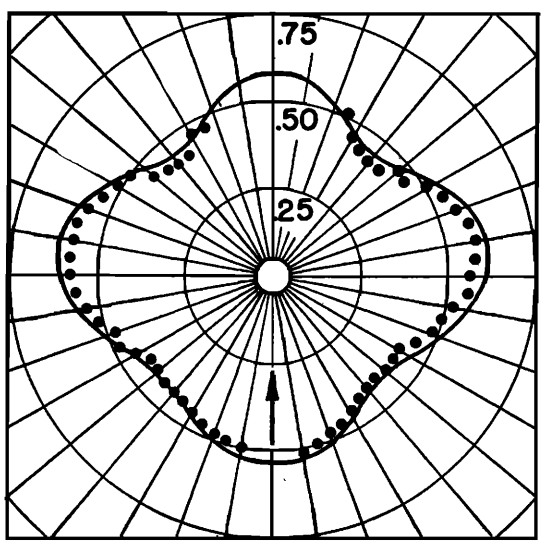

FIG. 4. Scattering pattern for steel cylinder 0.032 in. in diameter at 1.00 mc/sec. *Points:* Measured amplitude of pressure in the scattered wave. The measured Young's modulus was 20.0×10^{11} dynes/cm^2. *Curve:* Computed pattern for $x_3=1.7$, $x_1=0.45$, $\sigma=0.28$, $\rho_1=7.7$ g/cm^3.

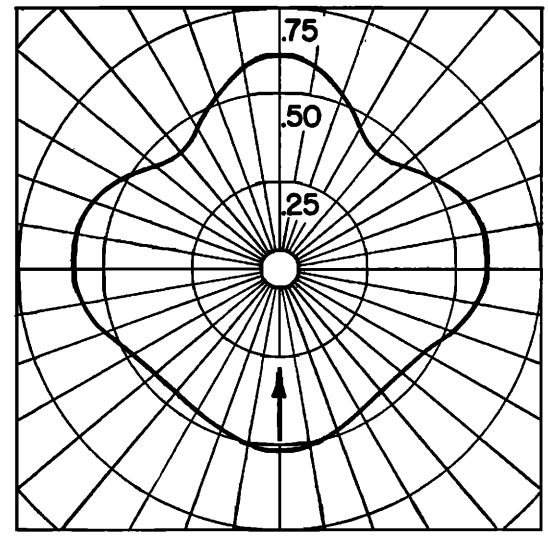

FIG. 5. Computed amplitude of pressure in wave scattered by a rigid, immovable cylinder for $x_3=1.7$.

(Fig. 6) is somewhat unusual; the amplitude of sound scattered back in the direction of the source is nearly zero. This near-null in the back-scattered sound is fully explained by the mathematical solution in which the

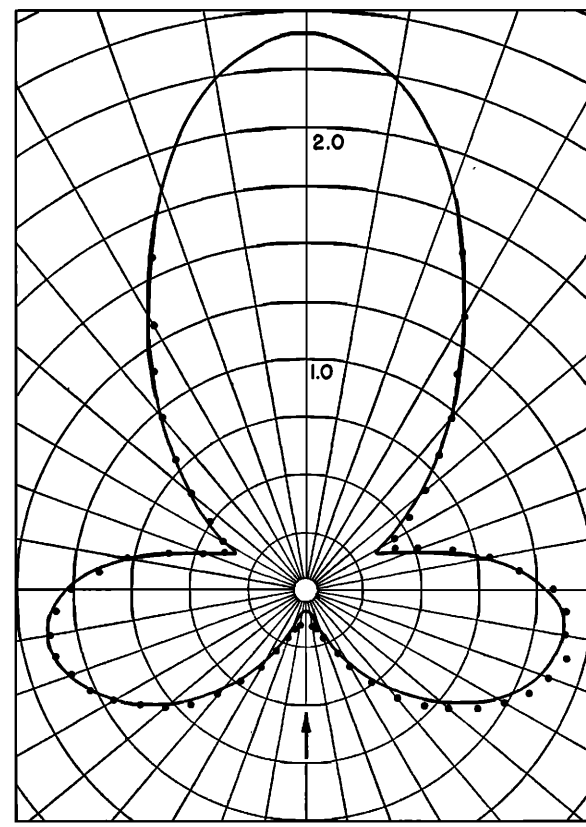

FIG. 6. Scattering pattern for brass cylinder 0.0625 in. in diameter at 1.02 mc/sec. *Points:* Measured amplitude of pressure in the scattered wave. The measured Young's modulus was 10.4×10^{11} dynes/cm^2. *Curve:* Computed pattern for $x_3=3.4$, $x_1=1.185$, $\sigma=\frac{1}{3}$, $\rho_1=8.5$ g/cm^3 (corresponding to $E=10.5\times 10^{11}$ dynes/cm^2).

term for $n=2$ in the series for the scattering pattern suddenly becomes very large in amplitude and of the proper phase to cancel the sum of all the other terms at $\theta=180°$. This, in turn, is brought about by the presence of an infinity in the $\tan\zeta_n(x_1, \sigma)$ function for $\sigma=\frac{1}{3}$ at $x_1=1.18\cdots$ (corresponding to a normal mode or resonance of the scatterer), in the neighborhood of which this function goes rapidly through a wide range of values causing the variations in the coefficient of the $n=2$ term. The value of x_1 for the computed pattern of Fig. 6 was chosen to give a deep notch at $\theta=180°$, and the frequency at which the experimental pattern was

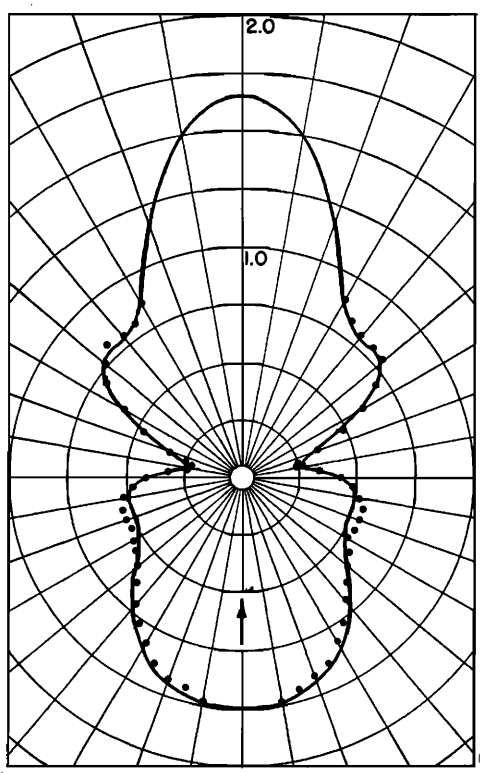

FIG. 7. Scattering pattern for copper cylinder 0.0625 in. in diameter at 1.00 mc/sec. *Points:* Measured amplitude of pressure in the scattered wave. The measured Young's modulus was 11.9×10^{11} dynes/cm². *Curve:* Computed pattern for $x_3=3.4$, $x_1=1.08$, $\sigma=\frac{1}{3}$, $\rho_1=8.9$ g/cm³ (corresponding to $E=12.7\times10^{11}$ dynes/cm²).

measured was chosen the same way. Figure 7 is the scattering pattern for a copper cylinder of the same size. The value of x_1 for the copper cylinder is near enough to 1.18 that the coefficient of the $n=2$ term is still large, but in this case it is of the opposite phase and causes the sound scattered in the direction $\theta=180°$ to be somewhat larger in amplitude than that scattered by a rigid, immovable cylinder of this size (Fig. 9). The velocity of sound in steel is so much higher than that in brass or copper that this scatterer behaves nearly as though it were rigid and immovable, and its scattering pattern (Fig. 8) is little different from that for the rigid, immovable case.

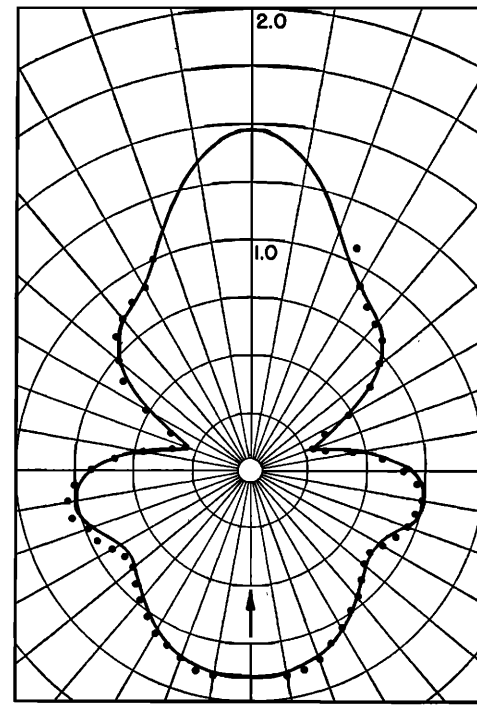

FIG. 8. Scattering pattern for steel cylinder 0.0625 in. in diameter at 1.00 mc/sec. *Points:* Measured amplitude of pressure in the scattered wave. The measured Young's modulus was 19.5×10^{11} dynes/cm². *Curve:* Computed pattern for $x_3=3.4$, $x_1=0.9$, $\sigma=0.28$, $\rho_1=7.7$ g/cm³.

Figures 10, 11, and 12 are scattering patterns for brass, steel, and aluminum cylinders for which $x_3=5.0$.

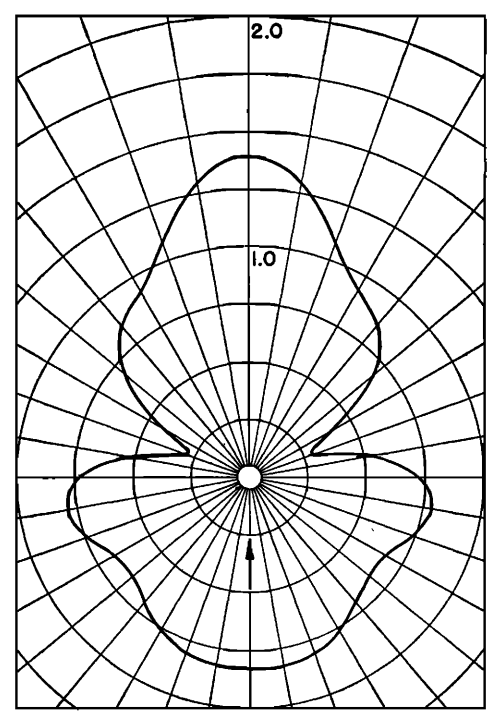

FIG. 9. Computed amplitude of pressure in wave scattered by a rigid, immovable cylinder for $x_3=3.4$.

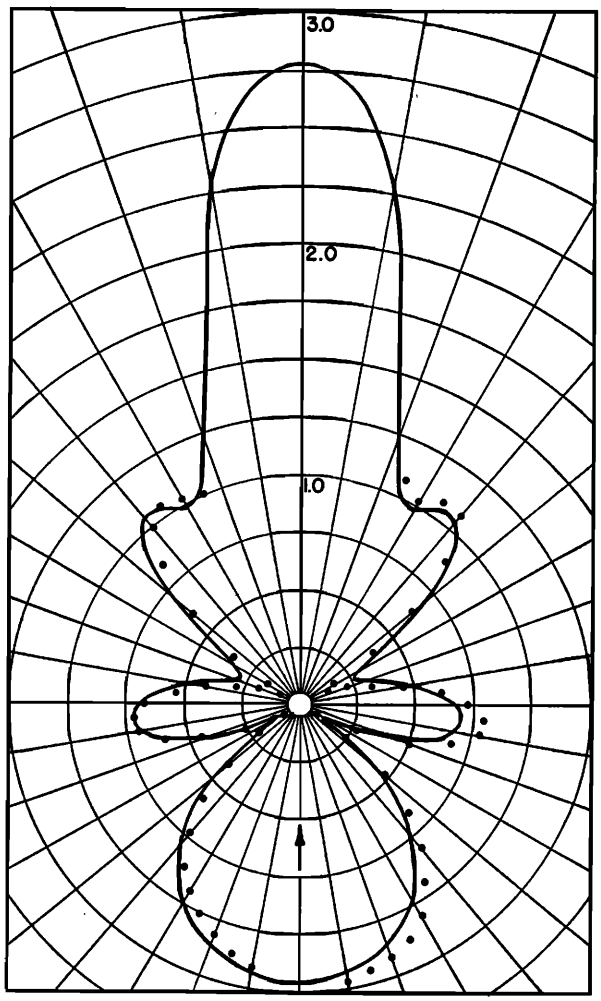

FIG. 10. Scattering pattern for brass cylinder 0.093 in. in diameter at 1.015 mc/sec. *Points:* Measured amplitude of pressure in the scattered wave. The measured Young's modulus was 10.0×10^{11} dynes/cm^2. *Curve:* Computed pattern for $x_3=5.0$, $x_1=1.78$, $\sigma=\frac{1}{3}$, $\rho_1=8.5$ g/cm^3 (corresponding to $E=10.2\times10^{11}$ dynes/cm^2).

The frequency of measurement of the pattern of the brass scatterer was chosen to give the deepest notch at 120°, and the value of x_1 was chosen to make the patterns agree. The choice of the value of x_1 is well substantiated by the measurement of the Young's modulus of this scatterer, since the value of E corresponding to the chosen value of x_1 is within 2 percent of the measured value. Figure 11 shows that, just as in the case of brass (Fig. 4), there is a near-null in the sound back-scattered from a steel cylinder at a frequency near that of the lowest-frequency normal mode which, for $\sigma=0.28$, occurs at $x_1=1.30\cdots$. Figure 12 shows that the same is true of an aluminum scatterer of the same size. Although the velocity of compressional waves in steel is not the same as that in aluminum, the values of Poisson's ratio differ sufficiently that this normal mode occurs in these two materials for the same physical size of the scatterers. These two patterns are so similar that they are seen to depend much more critically upon the value of x_1 than upon the density of the scatterer. The pattern for a rigid, immovable cylinder of the same size is shown in Fig. 13, and it is apparent that all these patterns for metal cylinders of this size bear little resemblance to this limiting case.

The theory thus verifies the existence of nulls in the back-scattered sound for cylinders of various metals, and at the proper frequencies; but a further test is to see whether it predicts properly the manner in which the amplitude of the back-scattered sound (and the shape of the entire pattern) changes with frequency. In order to test this, patterns were measured for the brass cylinder of Fig. 6 and the steel cylinder of Fig. 11 at two other frequencies, 3 percent below and above that at which the reference patterns were measured. The corresponding patterns predicted by the theory were computed by making a corresponding change in the values of the x parameters. In Fig. 14, the pattern of Fig. 6 is reproduced in the center, and those for 3 percent changes in frequency are shown at either side. In Fig. 15, the pattern of Fig. 11 is reproduced in the center, and the patterns for 3 percent changes in frequency are shown on either side. The theory is seen to predict the changes in the measured patterns with gratifying precision. These groups of patterns also emphasize the fact that the null

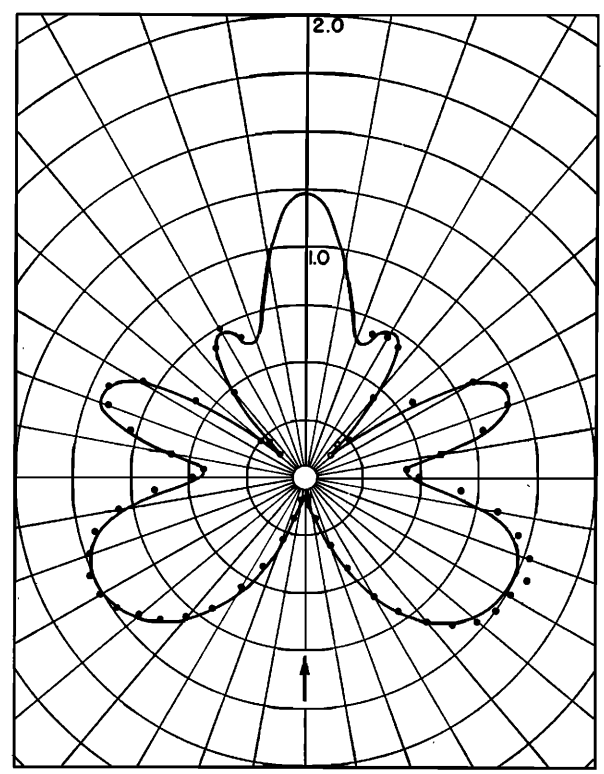

FIG. 11. Scattering pattern for steel cylinder 0.09375 in. in diameter at 0.99 mc/sec. *Points:* Measured amplitude of pressure in the scattered wave. The measured Young's modulus was 19.3×10^{11} dynes/cm^2. *Curve:* Computed pattern for $x_3=5.0$, $x_1=1.293$, $\sigma=0.28$, $\rho_1=7.7$ g/cm^3 (corresponding to $E=19.7\times10^{11}$ dynes/cm^2).

in the back-scattered sound is very sensitive to frequency.

Measurements of scattering by a few spheres were made with this apparatus. However, because the sound scattered by a sphere diverges in three dimensions (instead of two, as in the case of a long cylinder), the measurement was found to be very difficult, because of the reduced margin of signal to noise. The measurements (and also computations) indicate that, although rapid changes in the pattern do occur, there is no null in the sound back-scattered in water by a brass sphere, near its lowest-frequency normal mode of vibration.

V. REMARKS ON THE BEHAVIOR OF SOLID SCATTERERS

It is interesting to examine the behavior of certain of the functions which appear in the mathematical solution, especially the $\tan\zeta_n(x_1, \sigma)$ functions. As noted above, it can be shown that the infinities of the $\tan\zeta_n(x_1, \sigma)$ functions occur at precisely the frequencies of those normal modes of free vibration of the scattering body which satisfy the conditions of symmetry of the scattering problem. This can be done by applying boundary conditions to expressions for displacement and dilatation written in general form in terms of an unknown frequency. The boundary conditions, for free vibrations, are simply that the normal component of stress and the tangential components of shearing stress

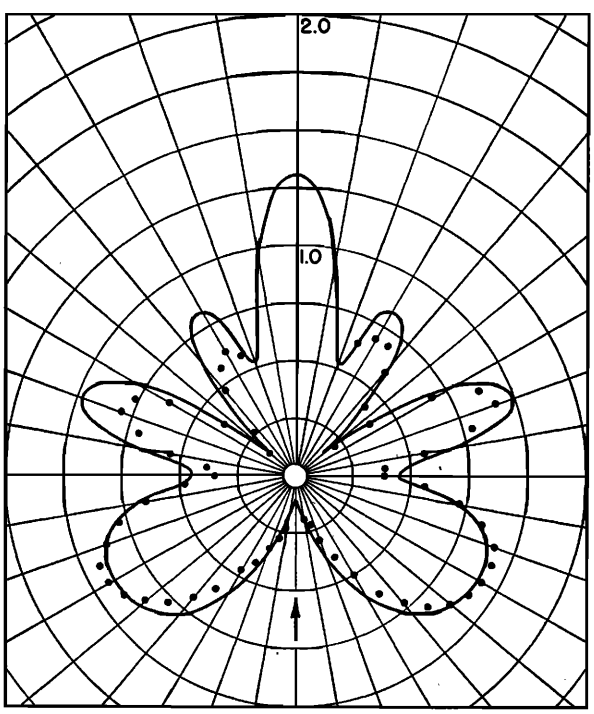

FIG. 12. Scattering pattern for aluminum cylinder 0.0925 in. in diameter at 1.00 mc/sec. *Points:* Measured amplitude of pressure in the scattered wave. The measured Young's modulus was 7.0×10^{11} dynes/cm². *Curve:* Computed pattern for $x_3=5.0$, $x_1=1.17$, $\sigma=\frac{1}{3}$, $\rho_1=2.7$ g/cm³ (corresponding to $E=7.2\times10^{11}$ dynes/cm²).

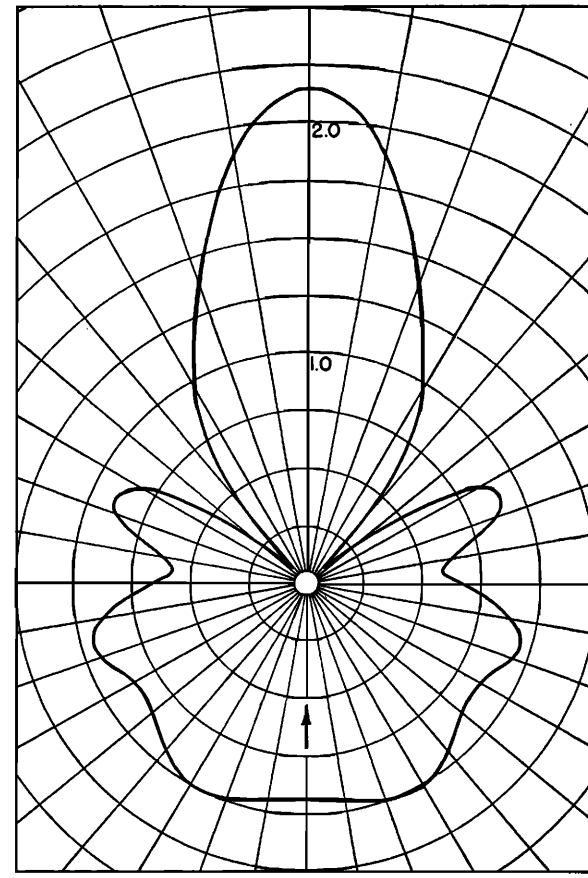

FIG. 13. Computed amplitude of pressure in wave scattered by a rigid, immovable cylinder for $x_3=5.0$.

at the surface of the body must both vanish. Solving the resultant equation for frequency (in terms of unknown x_1 and x_2 parameters) gives a condition which, in the cylindrical case, is identical to requiring the denominator of Eq. (24) to vanish.[10] For $\sigma=\frac{1}{3}$, the first few of these normal modes occur at the following values of the frequency parameter:

for $n=0$, $x_1=2.17\cdots$, $5.43\cdots$, $8.60\cdots$;
for $n=1$, $x_1=1.43\cdots$, $3.27\cdots$, $3.74\cdots$;
for $n=2$, $x_1=1.18\cdots$, $2.25\cdots$, $3.98\cdots$;
for $n=3$, $x_1=1.81\cdots$, $3.01\cdots$, $4.65\cdots$;
for $n=4$, $x_1=2.36\cdots$, etc.

The first normal modes for $n=1$, 2, and 3 occur for lower values of x_1 (lower frequencies) than that for $n=0$, contrary to what we might expect. The reason for this is that there are no shear waves associated with the $n=0$ normal modes. The complicated wave structure which comprises a normal mode can be realized at a much lower frequency with shear waves than without, because the velocity of shear waves is so much lower than that of compressional waves.

For fluid scatterers, the functions $\tan\zeta_n(x_1, \sigma)$ in Eqs. (23) and (29) are replaced[3] by the functions

[10] For details of this demonstration, see reference 9.

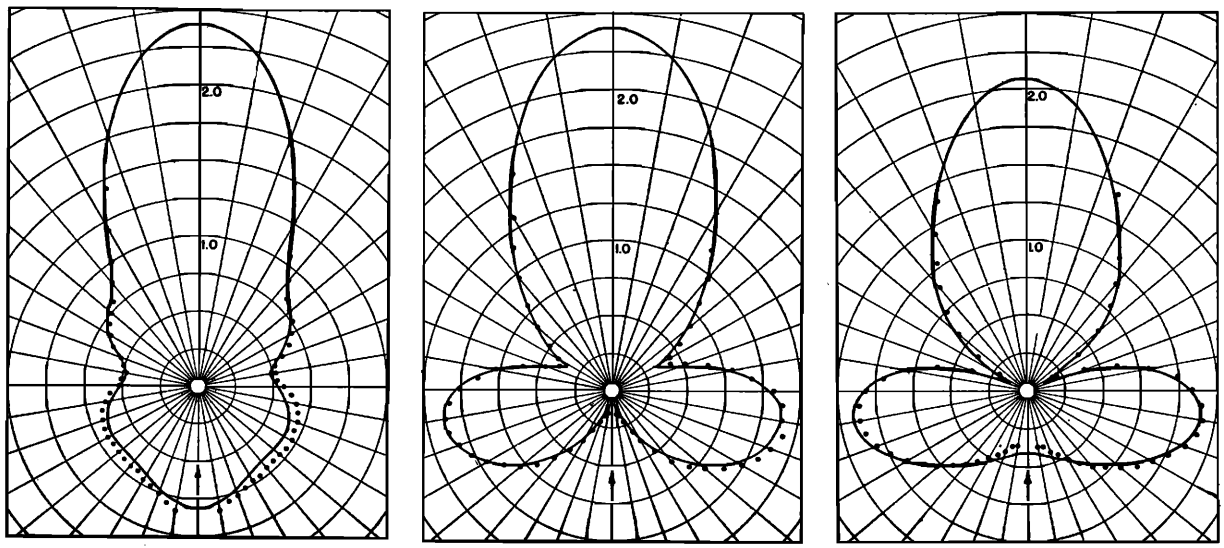

FIG. 14. The scattering pattern of Fig. 6 repeated for comparison with measured and computed patterns for frequencies 3 percent higher (right) and 3 percent lower (left).

$\tan\alpha_n(x_1)$. It is interesting to note that the infinities of these functions also correspond to frequencies of normal modes of free vibration of the (fluid) scatterer, since the infinities of $\tan\alpha_n(x_1)$ occur at the zeros of $J_n(x_1)$ or $j_n(x_1)$, in the cylindrical and spherical cases, respectively.

The coefficient c_n in the series for the scattering pattern does not attain its maximum value at exactly the frequencies of the normal modes of free vibration of the scatterer. Since the amplitude of c_n is proportional to $\sin\eta_n$, c_n reaches its maximum value when $\tan\eta_n$ becomes infinite. This represents a shift in the resonant frequency of the normal mode, and this shift is attributed to the reactive component of the acoustic impedance presented to the scatterer by the surrounding fluid, i.e., the reactive component of the radiation loading. In the case of solids having densities greater than that of the surrounding fluid, however, this frequency shift is usually small.

While measurements were being made with the experimental apparatus at frequencies near that of a normal mode, it was in some cases possible to observe "ringing" of that normal mode following the end of the pulse; that is, long transients could be observed at the end (and at the beginning) of the scattered pulse. By adjusting the frequency to give the maximum amplitude of the transient at the end of the pulse, it was thus possible to measure the frequencies of various normal modes. It was also possible to identify the order n of the excited mode, because the amplitude of the transient following the pulse was proportional to $\cos n\theta$. These transients were not noticeable in the case of the first normal mode for $n=2$. Apparently the damping by

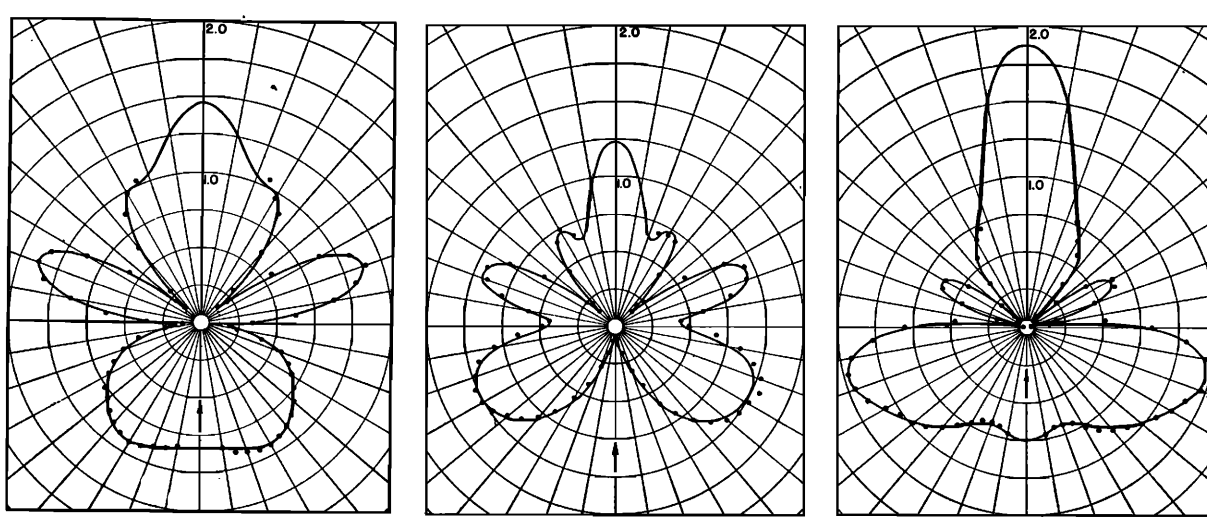

FIG. 15. The scattering pattern of Fig. 11 repeated for comparison with measured and computed patterns for frequencies 3 percent higher (right) and 3 percent lower (left).

radiation into the water was great enough to cause any ringing to die out quickly. However, the first normal modes for $n=0$, 1, and 3 were observed and identified for brass and steel cylindrical scatterers of appropriate sizes and showed good agreement with the frequencies predicted by the theory.

That there are sizeable shifts in the frequencies of the normal modes with changes in Poisson's ratio suggests that finding the frequencies of one or more of these normal modes of vibration might provide a method of measuring Poisson's ratio for cylindrical or spherical specimens. The variation of the frequencies of these normal modes with Poisson's ratio is illustrated in Figs. 16 and 17, where the values of x_1 at which the first normal modes for $n=0$, 1, 2, 3, and 4 occur are plotted as functions of Poisson's ratio. The variation of the second normal mode for $n=2$ is also shown in the graph for the spherical case. In this connection, as well as in the scattering problem itself, the potential utility of having the $\zeta_n(x_1, \sigma)$ functions computed for a wide range of values of Poisson's ratio will be evident. A computation program to yield these results appears to be justified. The frequencies of the normal modes cannot be computed explicitly, but can be found easily from the locations of the infinities of the $\tan\zeta_n(x_1, \sigma)$ functions.

It is interesting to compare the behavior of the $\tan\Phi_n$ functions for solid and fluid scatterers as x_1, the frequency parameter for the scatterer, approaches zero. For solid scatterers, either cylindrical or spherical, as $x_1 \to 0$,

$$\tan\Phi_n \to 0, \quad n \neq 1; \quad \tan\Phi_1 \to \rho_3/\rho_1;$$

while for fluid scatterers, where

$$\tan\Phi_n = (-\rho_3/\rho_1)\tan\alpha_n(x_1),$$

as $x_1 \to 0$,

$$\tan\Phi_n \to (\rho_3/\rho_1)n.$$

In neither case, by letting $x_1 \to 0$, do we realize the case of the rigid, immovable scatterer where $\tan\Phi_n = 0$ for all n. In order that $x_1 = \omega a/c_1 \to 0$ at finite frequencies in the solid case, the velocities of both the compressional and shear waves must become infinite, and the scatterer does indeed become rigid. The only term where $\tan\Phi_n$ does not vanish is that for $n=1$. This deviation from the rigid, immovable case is simply due to oscillation of the scatterer as a whole in synchronism with the incident sound field. Thus, by setting $x_1 = 0$ in the solution given here for solid scatterers, we can calculate the scattering from a rigid, *movable* cylinder or sphere of density ρ_1. To pass to the case of the rigid, immovable scatterer, we must also require that the density of the scatterer become infinite. In the case of a fluid scatterer, as $x_1 \to 0$, only $\tan\Phi_0$ approaches the value for the limiting case of a rigid, immovable scatterer. For $n=1$, $\tan\Phi_n$ behaves in the same way as in the case of the solid scatterer, and represents oscillation of the scatterer in synchronism with the incident sound. Now, for fluid scatterers, in order that $x_1 \to 0$ at finite frequencies, it is necessary that

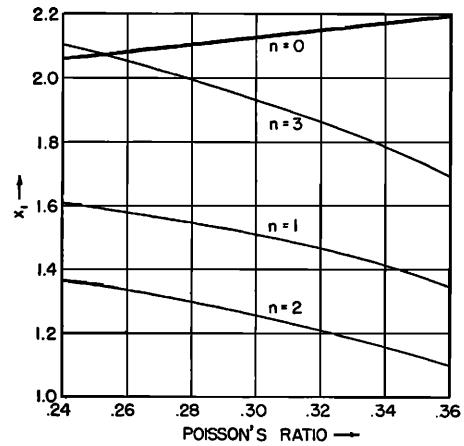

FIG. 16. The values of x_1 for the first few symmetrical normal modes of free vibration of a solid cylinder plotted as functions of Poisson's ratio.

the fluid become incompressible; but as this happens, the scatterer does not necessarily become rigid to shear distortions. It must then be that, for $n=2$ and higher, shape distortions of the incompressible fluid scatterer make the components of the scattered wave different from what they would be if the scatterer were rigid. Because the fluid scatterer never becomes rigid as $x_1 \to 0$, one can only pass from this solution to the case of the rigid, immovable scatterer by letting the density become infinite.

Two summary comments can be added regarding the general features of scattering by solid cylinders and spheres. If the frequency of the incident sound is lower than that of the first symmetrical normal mode of free vibration of the solid scatterer, and if the density of the scatterer is greater than that of the liquid, there is little difference between the scattering pattern for the solid scatterer and that for a rigid, immovable scatterer. But, rapid changes in the shape of the scattering pattern and in the total scattered power (or scattering cross section)

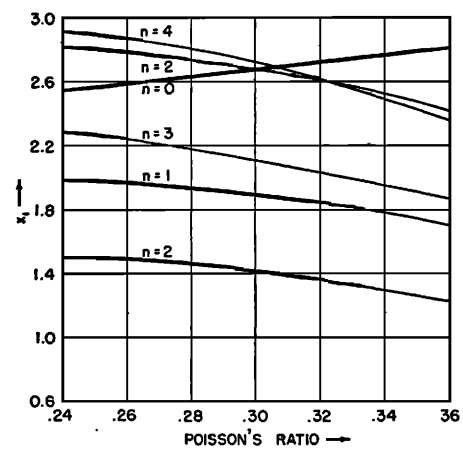

FIG. 17. The values of x_1 for the first few symmetrical normal modes of free vibration of a solid sphere plotted as functions of Poisson's ratio.

can occur with small changes in frequency in the vicinity of certain of the normal modes of free vibration of the solid scatterer. These changes include the appearance of deep minima in the scattering pattern at certain angles and may include, for cylinders, a near-null in the sound scattered back toward the source.

VI. ACKNOWLEDGMENTS

The author is indebted to Professor F. V. Hunt for his guidance and encouragement throughout this investigation. The assistance of Dorothea Greene, who performed the laborious computations for Figs. 16 and 17, is gratefully acknowledged.

THE JOURNAL OF THE ACOUSTICAL SOCIETY OF AMERICA VOLUME 23, NUMBER 4 JULY, 1951

The Growth of Subharmonic Oscillations

W. J. CUNNINGHAM
Yale University, New Haven, Connecticut
(Received January 14, 1951)

Subharmonic oscillations at one-half the frequency of excitation may appear in certain types of oscillating systems, among which is the direct-radiator loudspeaker. These oscillations occur at very nearly the resonant frequency of the system when the parameters of the system are made to vary at twice this frequency. The rate of growth of the subharmonic depends upon the amount of variation of the parameters relative to the dissipation in the system. If the dissipation is small, the rate of growth may be large. In the loudspeaker, conditions are such that the rate of growth is usually small for typical conditions of operation.

THE generation of subharmonic oscillations by a direct-radiator loudspeaker has often been observed.[1–4] Such oscillations usually occur at one-half the frequency of the current supplied to the loudspeaker, and appear for only certain discrete frequencies near the center of the audio spectrum. In most cases, the subharmonic is not present unless the loudspeaker is being operated near its maximum power. When present, the subharmonic is easily audible, even though sound pressure measurements indicate the amplitude of the subharmonic is only a few percent relative to the fundamental. The statement has been made that this subharmonic distortion is usually of little practical importance in the operation of the loudspeaker.[5] The reasoning is based on the observed fact that an appreciable length of time is required for the amplitude of the subharmonic to grow to its ultimate value. Since typical program material is of constantly changing nature, there is little opportunity for the subharmonic to build up. In the following rather simple discussion, the growth of the subharmonic oscillation is considered with the intent of determining what factors influence the rate of growth and why this rate is low for the loudspeaker.

Subharmonic oscillation at one-half the frequency of an exciting force may occur in oscillating systems having a single degree of freedom.[6,7] For the subharmonic to appear, the quiescent resonant frequency of the system must be very nearly one-half the exciting frequency. Further, operation must be such that under excitation the resonant frequency of the system is caused to vary at the exciting frequency. This variation must take place in such a way that sufficient energy is being supplied to the system to replace that lost by dissipation. If more than this amount of energy is supplied, the amplitude of the subharmonic grows, in theory, without limit. Ultimately, in practical systems, some additional effect takes over and the amplitude achieves a steady value.

In order to give a simple example of this type of operation, an electric circuit will be considered in some detail. This circuit contains in series combination an inductance L, a resistance R, and a capacitance C. If q is the instantaneous charge on the capacitance, the sum of voltages around the circuit is

$$L\ddot{q}+R\dot{q}+q/C=0, \tag{1}$$

where dots indicate time derivatives. In some way the capacitance is made to vary sinusoidally in time by an amount ΔC about the mean value C_0. The instantaneous capacitance is

$$C=C_0(1+a\sin 2\omega_1 t), \tag{2}$$

where the angular frequency of the variation is taken as $2\omega_1$, and $a\equiv\Delta C/C_0$. Evidently a can never exceed unity. It is possible to show that such a variation in capacitance can add energy to the oscillating circuit. The resonant angular frequency of the circuit in its quiescent

[1] H. F. Olson, *Acoustical Engineering* (D. Van Nostrand Company, Inc., New York, 1947), p. 167.
[2] P. O. Pederson, J. Acoust. Soc. Am. 6, 227–238 (1935), and 7, 64–70 (1935).
[3] F. von Schmoller, Telefunken Zeitung 67, 47–54 (June, 1934).
[4] G. Schaffstein, Hochfrequenztechn. Elektroakust. 45, 204–213 (1935).
[5] See reference 2. Also, H. S. Knowles, "Loudspeakers and room acoustics," Sec. 22, *Henney's Radio Engineering Handbook* (McGraw-Hill Book Company, Inc., New York, 1941), p. 902.
[6] N. Minorsky, *Nonlinear Mechanics* (Edwards Brothers, Inc., Ann Arbor, 1947), Chap. XIX.
[7] N. W. McLachlan, *Ordinary Nonlinear Differential Equations* (Oxford University Press, London, 1950), Chap. VII.